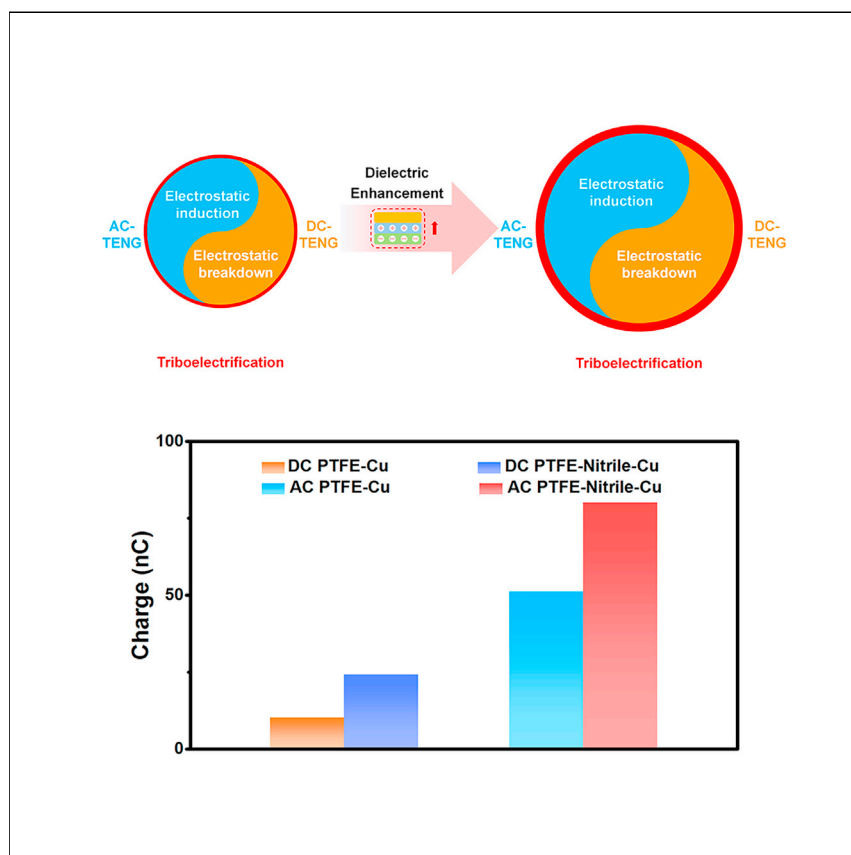


Article

Improving performance of triboelectric nanogenerators by dielectric enhancement effect



A dielectric enhancement effect is firstly proposed to improve the performance of triboelectric nanogenerators (TENGs) by elevating the triboelectrification effect. More importantly, the dielectric enhancement effect exhibits universality for all types of TENG. Moreover, the dielectric enhancement layer with leakage current is proven to be necessary for DC-TENG to produce continuous output. Through comparison experiments, output power of 8.5-fold enhancement for AC-TENG and 2.6-fold enhancement for DC-TENG are achieved compared with normal devices.

Shengnan Cui, Linglin Zhou, Di Liu, ..., Wei Yuan, Zhong Lin Wang, Jie Wang

zhong.wang@mse.gatech.edu (Z.L.W.)
wangjie@binn.cas.cn (J.W.)

Highlights

Dielectric enhancement effect is proposed for enhancing the performance of TENGs

Enhanced triboelectrification effect is verified as the mechanism of DE-TENG

The mechanism of DEDC-TENG producing sustained DC output is proposed

Dielectric enhancement effect is universal for all types of TENG



Improvement

Enhanced performance with innovative design or material control

Article

Improving performance of triboelectric nanogenerators by dielectric enhancement effect

Shengnan Cui,^{1,2,4} Linglin Zhou,^{1,2,4} Di Liu,^{1,2,4} Shaoxin Li,^{1,2} Li Liu,^{1,2} Shengyang Chen,^{1,2} Zhihao Zhao,^{1,2} Wei Yuan,^{1,2} Zhong Lin Wang,^{1,2,3,*} and Jie Wang^{1,2,5,*}

SUMMARY

As an emerging energy-harvesting technology, enhancing the output performance of triboelectric nanogenerators (TENGs) is crucial for its practical application. Here, a dielectric enhancement effect is firstly proposed to improve the output performance of TENGs. It is found that the dielectric enhancement layer greatly elevates the triboelectrification effect, and the enhanced performance is verified by all types of TENGs. Thus, the output power of alternative current TENG (AC-TENG) and direct current TENG (DC-TENG) realizes 8.5-fold and 2.6-fold enhancement of normal devices, respectively. Besides this, the dielectric enhancement layer with leakage performance is proven to be necessary for DC-TENG to produce a continuous output. Our work provides a simple and universal strategy for elevating the performance of all types of TENGs, which is beneficial to the promotion of large-scale energy harvesting by TENGs.

INTRODUCTION

As the world enters the era of the Internet of Things (IoT) and artificial intelligence, widely distributed and numerous sensors that form the foundation of the IoT are crucial for the collection of mass data information, and a continuous energy supply is an important requirement for the operation of these sensors.¹ Based on the combination of triboelectrification (TE) and electrostatic induction effects, the alternative current triboelectric nanogenerator (AC-TENG) was first invented by the Wang group in 2012 for the conversion of randomly distributed and ubiquitous mechanical energy into electricity.² With its advantages of light weight, broad materials availability, low cost, and high efficiency even when operating at low frequency, TENG exhibits great potential in the application of IoT and artificial intelligence in powering a wide number of sensors.^{3–9}

As an energy-harvesting device, the wide application of TENG depends on its power density, which is determined by the triboelectric charge density.^{10,11} Based on TE and electrostatic induction, the limited factors of the effective surface charge density of AC-TENG ($\sigma_{AC-TENG}$) can be described as follows:¹²

$$\sigma_{AC-TENG} = \min(\sigma_{\text{triboelectrification}}, \sigma_{r, \text{air breakdown}}, \sigma_{\text{dielectric breakdown}}). \quad (\text{Equation 1})$$

Researchers have invested great efforts in increasing the $\sigma_{\text{triboelectrification}}$ such as material optimization,¹³ ion injection,¹⁴ and surface modification.¹⁵ Nevertheless, with the increase of the surface charge density on the surface of dielectric film, the output of AC-TENG will be limited by air breakdown. Recently, some strategies including a high vacuum environment¹² and an ultrathin dielectric film¹⁶ were proposed to avoid air breakdown and thus further improve the $\sigma_{r, \text{air breakdown}}$. In addition, to break

Progress and potential

The triboelectric nanogenerator (TENG) is a burgeoning energy-harvesting technology, and enhancing its output performance is essential for practical application. In this work, a simple and universal method has been developed to improve the output performance of TENGs by a dielectric enhancement effect. The universality of the dielectric enhancement layer for TENG is verified by comparison experiments for all types of TENG. Furthermore, the mechanism of dielectric enhanced DC-TENG (DEDC-TENG) producing sustained DC output is proposed and analyzed, which comprises breakdown electrons passing through the dielectric enhancement film to the dielectric layer in the form of leakage current. This work provides a simple and universal strategy for elevating the performance of all types of TENG, which is beneficial to promoting TENGs for large-scale energy harvesting.

through the limitation of $\sigma_{\text{triboelectrification}}$, external circuit optimization^{17–20} is an effective strategy to boost the surface charge density.

To utilize the air breakdown, the direct current TENG (DC-TENG) was auspiciously invented by coupling the effects of TE and the electrostatic breakdown effect, which can effectively harvest mechanical energy to directly drive electronic devices without any auxiliary rectifiers and energy-storage units.²¹ Based on the working mechanism of DC-TENG, the limited factors of the effective surface charge density of DC-TENG ν ($\sigma_{\text{DC-TENG}}$) can be described as follows:²²

$$\sigma_{\text{DC-TENG}} = k \times \min(\sigma_{\text{triboelectrification}}, \sigma_{\text{c, electrostatic breakdown}}). \quad (\text{Equation 2})$$

To date, many efforts have been devoted to improving the surface charge density of DC-TENG. High temperature, an appropriate low atmospheric pressure, and atmosphere control can improve the output performance of DC-TENG by increasing the $\sigma_{\text{c, electrostatic breakdown}}$.^{23,24} Additionally, microstructure design is another way to improve $\sigma_{\text{DC-TENG}}$ by a high k value.²² Aiming to elevate the surface charge density of both AC-TENG and DC-TENG, an effective strategy via interface liquid lubrication was proposed by suppressing interface breakdown and improving the efficiency of TE.²⁵ According to Equations 1 and 2, the surface charge density of AC-TENG and DC-TENG can be both enhanced by improving the TE and thereby the output performance of TENGs can be boosted.

In this work, we propose a new method to improve the output performance of TENGs by a dielectric enhancement effect (defined as using dielectric material to improve the TENG's performance). By incorporating a dielectric enhancement layer on the friction electrode, the dielectric enhanced TENG (DE-TENG) can increase the TE and thus achieve a higher output value of TENGs. The enhanced performance of the dielectric enhancement effect is verified by all types of TENGs. By using the dielectric enhancement layer, the output power of AC-TENG and DC-TENG realizes 8.5-fold and 2.6-fold enhancement of normal devices, respectively. In addition, the mechanism of dielectric enhanced DC-TENG (DEDC-TENG) producing sustained DC output is proposed and analyzed, whereby breakdown electrons pass through the dielectric enhancement film to the dielectric layer in the form of leakage current. For demonstration purposes, a rotary dielectric enhanced AC-TENG (DEAC-TENG) and DEDC-TENG are fabricated to harvest environmental energy for charging a capacitor and powering an electronic device. This work provides a simple and universal strategy to elevate the performance of all types of TENG.

RESULTS AND DISCUSSION

Dielectric enhancement effect for TENGs

A TENG is an effective strategy to convert mechanical energy into electrical energy. In principle, TENG can be divided into AC-TENG and DC-TENG. As an energy-harvesting technology, the energy flow chart of TENG can be summarized as follows (Figure 1A): TE converts mechanical energy into electrostatic energy, whereby AC-TENG can convert electrostatic energy to AC output via electrostatic induction, while DC-TENG can directly transform electrostatic energy to DC output via electrostatic breakdown without any rectification methods (Figure 1B). Therefore, the output performance of AC-TENG and DC-TENG can be simultaneously improved through enhancement of TE.

Here, nitrile is used as a dielectric enhancement layer for improving the TE, and thus elevates the performance of both AC-TENG and DC-TENG (Figure 1A), which has been demonstrated by dual-mode TENG. The three-dimensional (3D) structure of

¹Beijing Institute of Nanoenergy and Nanosystems, Chinese Academy of Sciences, Beijing 100083, P. R. China

²College of Nanoscience and Technology, University of Chinese Academy of Sciences, Beijing 100049, P. R. China

³School of Materials Science and Engineering, Georgia Institute of Technology, Atlanta, GA 30332, USA

⁴These authors contributed equally

⁵Lead contact

*Correspondence:
zhong.wang@mse.gatech.edu (Z.L.W.),
wangjie@binn.cas.cn (J.W.)

<https://doi.org/10.1016/j.matt.2021.10.019>

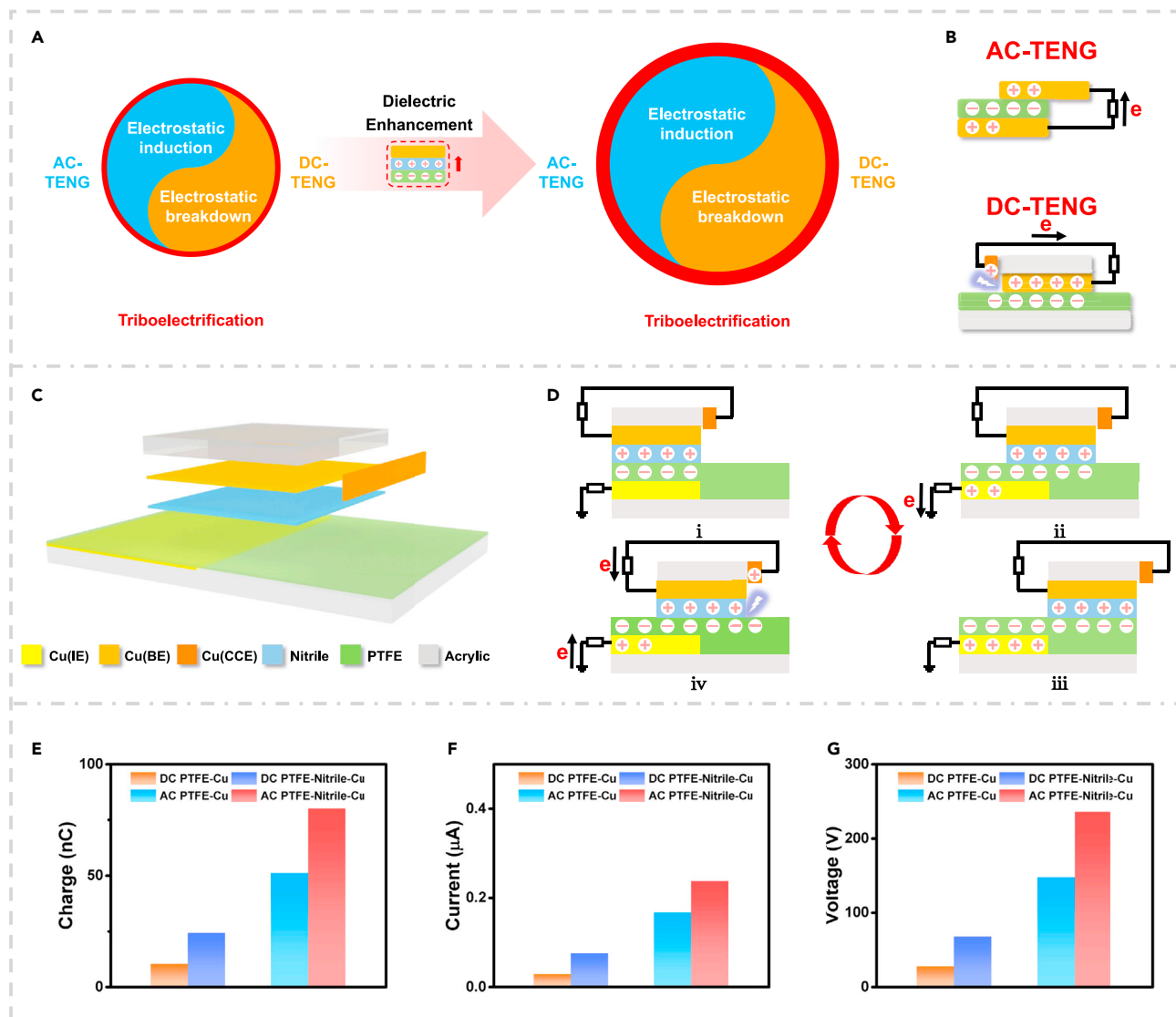


Figure 1. Structure and working mechanism of TENG with dielectric enhancement layer

(A) Energy conversion diagram of AC-TENG and DC-TENG.

(B) Characteristics of AC-TENG and DC-TENG.

(C) Schematic illustration of dual-mode dielectric enhanced TENG.

(D) Working mechanism of dual-mode dielectric enhanced TENG.

(E–G) Output charge (E), short-circuit current (F), and open-circuit voltage (G) comparison of dual-mode dielectric enhanced TENG and normal dual-mode TENG.

the dual-mode TENG with a dielectric enhancement layer is schematically illustrated in Figure 1C, which mainly contains a stator and a slider working in the sliding status. The stator consists of an induction electrode (IE) connected to polytetrafluoroethylene (PTFE) as triboelectric layer.²⁶ The sliding part is composed of a back electrode (BE), a charge collecting electrode (CCE), and nitrile as dielectric enhancement layer.²⁷ The detailed fabrication process is described in [experimental procedures](#).

The principle of dual-mode DE-TENG is based on TE, electrostatic induction, and electrostatic breakdown. As shown in Figure 1D, the whole working cycle can be divided into four stages. In the initial state, PTFE and nitrile come into physical

contact and carry the opposite electric charges due to TE. As the slider moves to the right in the horizontal direction, there will be a potential difference between IE and BE. To balance the potential difference, a current signal will appear in the external circuit, which always exits until the slider moves to the edge of the IE electrode. When the slider moves back, there will be an opposite current signal due to the reverse flow of electrons. At the same time, PTFE can preserve the negative charges on the surface due to the electret effect. Therefore, as the slider moves to the left, there will be a high electric field between PTFE and CCE. Once the value of electric field exceeds 3 kV mm^{-1} , the surrounding air will be ionized and the negative charges on the PTFE surface will transfer to the CCE. The charges then flow from CCE to BE via the external circuit. Based on the aforementioned, the whole cycle motion can produce both DC and AC signals.

To measure the effect of the dielectric enhancement effect on the output performance of dual-mode TENG, the devices are driven by a linear motor separately for horizontal sliding movement. The ordinary dual-mode TENG consists of IE, dielectric layer (here PTFE), friction electrode (FE), and CCE (Figure S1A). Comparisons of the charge, short-circuit current, and open-circuit voltage of two devices are shown in Figures 1E–1G and S1B–S1D. Obvious higher output of the dual-mode TENG is observed by using the dielectric enhancement layer. The transferred charges of DC increase from 10 nC to 24 nC, an enhancement of 140%, while the transferred charges of AC increase from 51 nC to 80 nC or 57% enhancement. Moreover, the short-circuit current and open-circuit voltage exhibit similar increasing tendency. The short-circuit current and open-circuit voltage of DC increase from 0.027 to 0.074 μA and from 27 to 67 V, respectively, while the short-circuit current and open-circuit voltage of AC increase from 0.165 to 0.236 μA and from 147 to 235 V, respectively.

Universality of the dielectric enhancement effect for TENGs

To further verify the universality of the dielectric enhancement effect for TENGs, we also compared the output performance of traditional AC-TENG and DC-TENG with the corresponding DEAC-TENG and DEDC-TENG. Based on the working mode, traditional AC-TENG can be classified into vertical contact-separation mode (CS), single-electrode mode (SE), sliding freestanding triboelectric-layer mode (SFT), and sliding mode (SL) (Figures S2A–S2D). For these four modes of AC-TENG the surface of two dissimilar materials takes opposite charges due to TE. When the separation distance or contact area of these two materials changes with a reciprocating motion, an induced potential difference will be generated, resulting in an alternative current in the external circuit. The detailed working mechanisms of these four AC-TENGs are depicted in Note S1. The structures of four types of DEAC-TENG are depicted in Figures 2A, 2E, 2I, and 2M, where the main difference in structure compared with the traditional TENGs is that all of them have a dielectric enhancement layer on the FE.

The comparison of the transferred charges, short-circuit current, and open-circuit voltage between DEAC-TENG and AC-TENG are shown in Figures 2B–2D, 2F–2H, 2J–2L, and 2N–2P. The transferred charges of four modes DEAC-TENGs (CS-mode DEAC-TENG, SE-mode DEAC-TENG, SFT-mode DEAC-TENG, and SL-mode DEAC-TENG) are 12.4 nC, 10.7 nC, 74.1 nC, and 59.6 nC, increases of 16%, 49%, 42%, and 62%, respectively compared with normal AC-TENGs. Additionally, the short-circuit current and open-circuit voltage of the four modes of DEAC-TENG exhibit similar increasing tendency with the transferred charge as displayed in Figures 2C–2D, 2G–2H, 2K–2L, and 2O–2P. These results demonstrate the

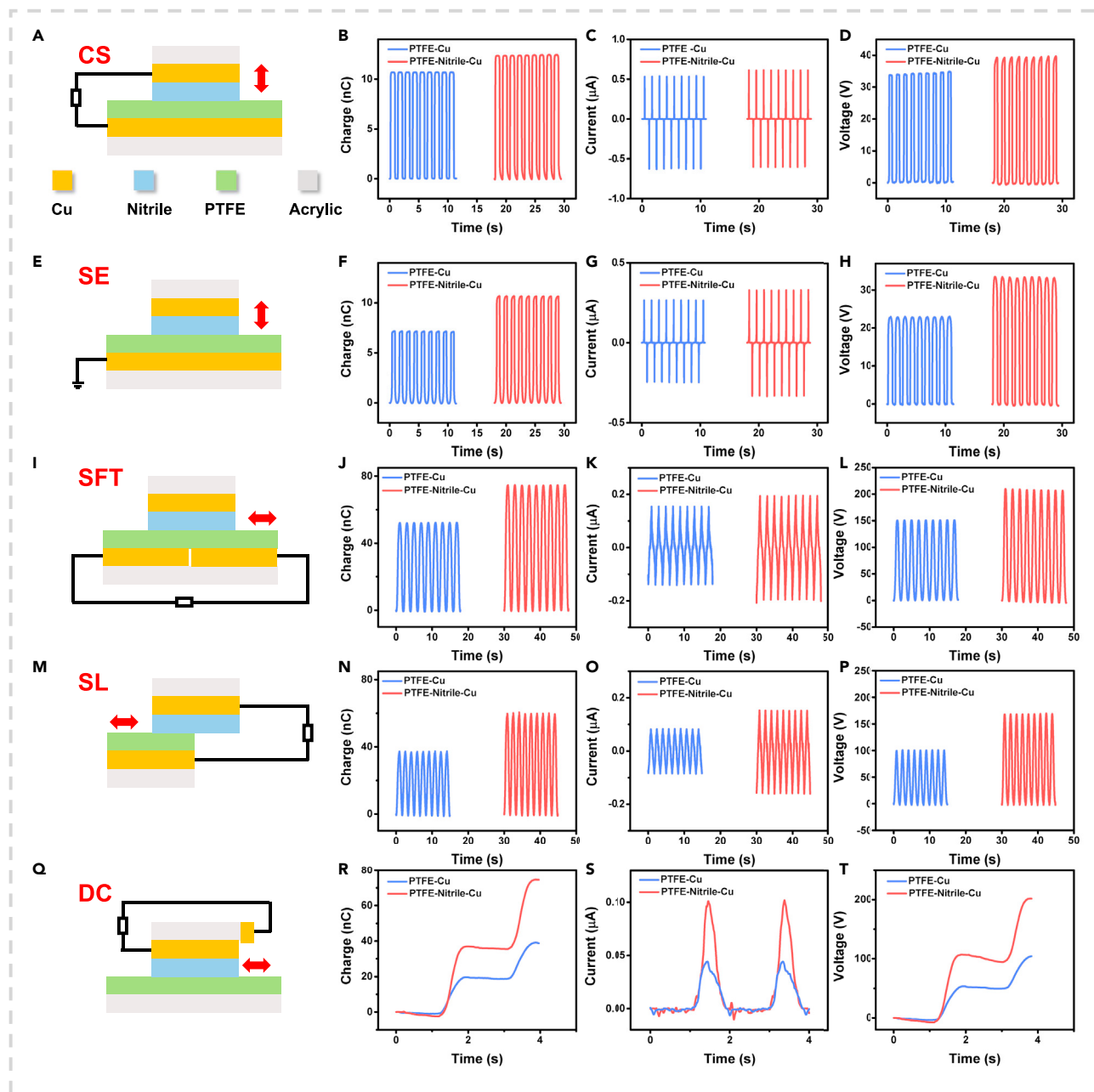


Figure 2. Output performance of several types of DE-TENG

(A) Schematic illustration of CS-mode DEAC-TENG.

(B–D) Output charge (B), short-circuit current (C), and open-circuit voltage (D) comparison of CS-mode DEAC-TENG and normal CS-mode AC-TENG.

(E) Schematic illustration of SE-mode DEAC-TENG.

(F–H) Output charge (F), short-circuit current (G), and open-circuit voltage (H) comparison of SE-mode DEAC-TENG and normal SE-mode AC-TENG.

(I) Schematic illustration of SFT-mode DEAC-TENG.

(J–L) Output charge (J), short-circuit current (K), and open-circuit voltage (L) comparison of SFT-mode DEAC-TENG and normal SFT-mode AC-TENG.

(M) Schematic illustration of SL-mode DEAC-TENG.

(N–P) Output charge (N), short-circuit current (O), and open-circuit voltage (P) comparison of SL-mode DEAC-TENG and normal SL-mode AC-TENG.

(Q) Schematic illustration of DEDC-TENG.

(R–T) Output charge (R), short-circuit current (S), and open-circuit voltage (T) comparison of DEDC-TENG and normal DC-TENG.

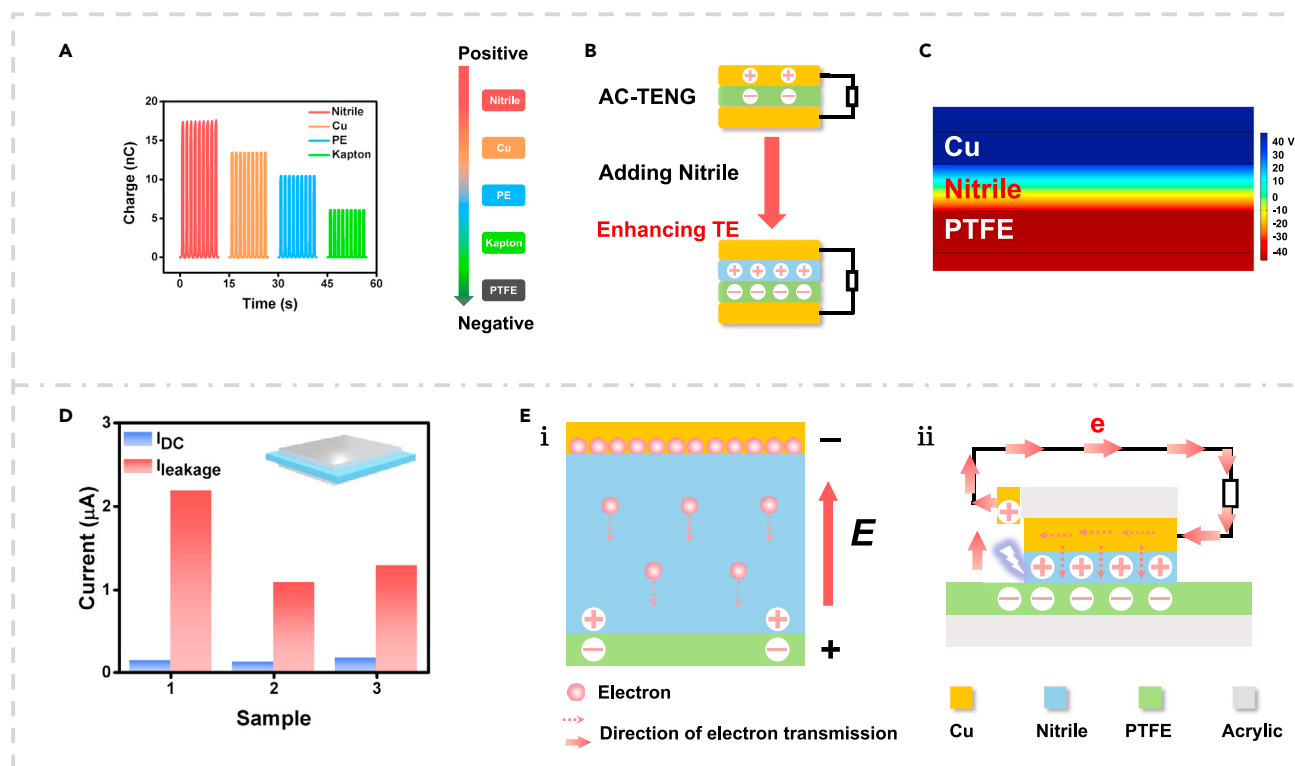


Figure 3. Working mechanism of dielectric enhancement effect for improving the performance of TENG

- (A) Transfer charge of nitrile, Cu, PE, and Kapton with PTFE.
 (B) Working mechanism of improving the performance of AC-TENG by dielectric enhancement effect.
 (C) Potential distribution between dielectric layers of DC-TENG.
 (D) Comparison of leakage of nitrile and current of DEDC-TENG.
 (E) Working mechanism of DEDC-TENG.

improved output performance of four modes AC-TENG by the dielectric enhancement method.

We also compared the output performance of DEDC-TENG and the normal DC-TENG. The structures of DEDC-TENG and DC-TENG are displayed in [Figures 2Q](#) and [S2E](#), and the working mechanism of DC-TENG is described in [Figure S2F](#) and [Note S2](#). As depicted in [Figures 2R–2T](#), the DEDC-TENG can generate a good DC output signal, and its transferred charge, short-circuit current, and open-circuit voltage are 39.4 nC, 0.101 μA , 113.5 V, representing increases of by 90%, 129%, 101%, respectively compared with the normal DC-TENG. Furthermore, the effect of the gap between nitrile and CCE on output performance of DEDC-TENG was studied. As shown in [Figures S3](#) and [S4](#), the charge density decreases with the increase of the gap between nitrile and CCE ([Note S3](#)). Based on the above analyses, the improved output performance of all types of DE-TENG verifies the universality of the dielectric enhancement effect for all modes of TENG.

Mechanism of the dielectric enhancement effect

Although the position of nitrile in the triboelectric series has been mentioned in a previous review, the specific properties of nitrile as triboelectric material are not clear.²⁸ To investigate the mechanism of the dielectric enhancement effect, we used PTFE as the counter triboelectric layer to measure its transfer charges with nitrile, Cu, polyethylene (PE), and Kapton. As depicted in [Figure 3A](#), transferred

charges between nitrile and PTFE are much larger than that of Cu, PE, and Kapton, which indicates that the ability to lose negative charges of nitrile from PTFE is higher than that of Cu. The result demonstrates that using nitrile as the dielectric enhancement layer can largely improve the TE, thus enhancing the output performance of both AC-TENG and DC-TENG (Figure 3B).

We also investigated the mechanism of DC-TENG to generate a continuous DC output in the presence of a dielectric enhancement layer. For DC-TENG, the breakdown electrons pass through the circuit to reach FE and then transfer to the dielectric layer to produce continuous TE. However, there is a dielectric enhancement layer between FE and the triboelectric layer of the DEDC-TENG, so how do electrons get from the BE to the triboelectric layer? Considering the poor insulation performance of nitrile, we tested the leakage current of nitrile. Firstly the potential distribution of the dielectric layer was theoretically simulated by COMSOL Multiphysics software. According to the experimental data, we set the surface charge density of PTFE to $90 \mu\text{C m}^{-2}$, and the potential difference between both sides of nitrile is 60 V as depicted in Figure 3C. Based on the potential difference obtained by theoretical simulation, a 60 V bias voltage was applied to the silver-plated nitrile on both sides with a leakage current meter. As shown in Figure 3D, the leakage current of nitrile exceeds 1 μA , which is higher than the output current of the DEDC-TENG (Figure S5), indicating that electrons can pass through the nitrile in the form of leakage current. We also studied the behavior of charge dissipation in a real TENG by using nitrile-PTFE and PTFE-Cu as the triboelectric pairs. The faster charge loss behavior, higher initial surface charges, and higher stable surface charges in nitrile-PTFE again demonstrated the dielectric enhancement effect in DE-TENG (Figure S6 and Note S4). For DEDC-TENG, the breakdown electrons pass through the circuit to reach BE and accumulate, which strengthens the electric field applied on both sides of the nitrile and thus increases the leakage current (Figure 3Ei). Finally, a complete loop is formed. Based on the theoretical simulation and experimental results, the working mechanism of DEDC-TENG is displayed in Figure 3Eii. The DC-TENG is based on the principle of TE and electrostatic breakdown to generate a DC output, after which the breakdown electrons pass through the nitrile film to the dielectric layer in the form of leakage current to produce continuous DC output.

To demonstrate the universality of the dielectric enhancement effect, we chose thermoplastic polyurethane (TPU) and nylon as the dielectric enhancement layers. The corresponding output performance of CS-mode DEAC-TENG and DEDC-TENG are shown in Figures S7A and S7B. The results indicate that both TPU and nylon can improve the TE and thereby increase the output performance of DEAC-TENG and DEDC-TENG. We also tested the leakage current of silver-plated TPU and silver-plated nylon with a leakage current meter (the bias voltage is theoretically simulated by COMSOL and the surface charge density refers to the experimental data), as depicted in Figures S7C and S7D. The leakage currents of TPU and nylon both exceed their output current of the corresponding DEDC-TENG. In addition, by replacing the triboelectric layer with PE, whose leakage current is only around 1 nA, the output current of DEDC-TENG cannot continue to exist stably. As shown in Figure S7E, the output charges of normal DC-TENG are almost unchanged after 20 cycles, while DEDC-TENG with PE as triboelectric layer declines rapidly and even drops by 81.2% after 100 cycles compared with the initial value. The leakage current of silver-plated PE is measured with a leakage meter (the bias voltage is theoretically simulated by COMSOL as depicted in Figure S7F, and the surface charge density refers to the experimental data). The leakage current of PE is only 1 nA, which is inferior to the output current of the DEDC-TENG (Figure S7G). Therefore, the electrons

cannot pass through the PE to generate a continuous DC output, which also demonstrates the working mechanism of DEDC-TENG in this work from the opposite perspective. Otherwise, we use Al instead of Cu as the BE and CCE. The output performance of DEDC-TENG and DC-TENG is depicted in [Figure S7H](#). The enhanced result of DEDC-TENG indicates that the part of Cu can be replaced by Al as BE, further demonstrating the universality of the dielectric enhancement effect.

According to the above experimental results, there are two characteristics that the dielectric enhancement layer must possess to realize the dielectric enhancement effect: improved triboelectrification and permitting certain charges to be transferred in the form of leakage current. The former ensures improved performance in all types of TENG, while the latter aims to ensure the formation of an electric loop in DEDC-TENG to enhance the output performance of DEDC-TENG.

Output performance and application of rotary mode DE-TENG

To further demonstrate the enhanced output performance of DE-TENG and facilitate its application, we fabricated a rotary mode DEAC-TENG and DEDC-TENG ([Figures S8A](#) and [S10A](#), respectively). The 3D structure of rotary mode DEAC-TENG is depicted in [Figure 4A](#). The device is composed of a stator and slider. Both the stator and the slider consist of radially arrayed sectors, and each unit is similar to the SFT mode. The slider contains a copper foil as top electrode with a piece of nitrile pasted on it as positive triboelectric layer. The stator contains conductive fabrics as bottom electrodes and a piece of PTFE pasted on it as negative triboelectric layer.

Before the comparative experiment, the influence of rotation speed of DEAC-TENG was investigated. As shown in [Figures S8B–S8D](#), with the rotation speed changing from 100 r min^{-1} to 300 r min^{-1} , the transferred charges maintain a stable value while the short-circuit current and voltage increase from 4.6 to $16.8 \mu\text{A}$ and from 490 to 1148 V , respectively. The comparison of output performance between rotary mode AC-TENG and rotary mode DEAC-TENG at 300 r min^{-1} is shown in [Figures S8E–S8G](#). The transferred charges, the short-circuit current, and voltage of the rotary mode DEAC-TENG are all higher than that of the rotary mode AC-TENG, where the transferred charges increased by 137%. When connected to an external load, the current value of the two devices is almost stable, with the load resistance increasing from 0.001 to $30 \text{ M}\Omega$ and then declining from 100 to $400 \text{ M}\Omega$ ([Figure S8H](#)). Meanwhile, the maximal power output of rotary mode AC-TENG and rotary mode DEAC-TENG reach 1.33 and 12.64 mW ([Figure S8H](#)), respectively. The maximal power output of DEAC-TENG increased by 8.5-fold compared with normal devices. Furthermore, the voltage curves of capacitors with capacitance of $1.1 \mu\text{F}$, $2.2 \mu\text{F}$, and $4.7 \mu\text{F}$ charged by rotary mode AC-TENG and DEAC-TENG with a full-wave rectifier are depicted in [Figures 4B](#) and [4C](#). For charging the $1.1 \mu\text{F}$, $2.2 \mu\text{F}$, and $4.7 \mu\text{F}$ capacitors to 10 V , the rotary mode AC-TENG takes 3.45 s , 7.14 s , and 16.7 s , while the rotary mode DEAC-TENG takes 1.48 s , 2.94 s , and 6.23 s , respectively. The results indicate that the rotary mode DEAC-TENG takes less time than the rotary mode AC-TENG to charge the same capacitor.

The 3D structure of the rotary mode DEDC-TENG is depicted in [Figure 4D](#). The stator contains many sectors, each unit comprising BE, CCE, and nitrile, which is similar to the sliding mode DEDC-TENG; the CCE and BE are all connected together in parallel. The slider is composed of PTFE and a piece of foam to ensure contact intimacy between triboelectric layers. The influence of rotation speed in rotary mode DEDC-TENG is shown in [Figures 4E](#), [S10B](#), and [S10C](#). With the rotation speed changing

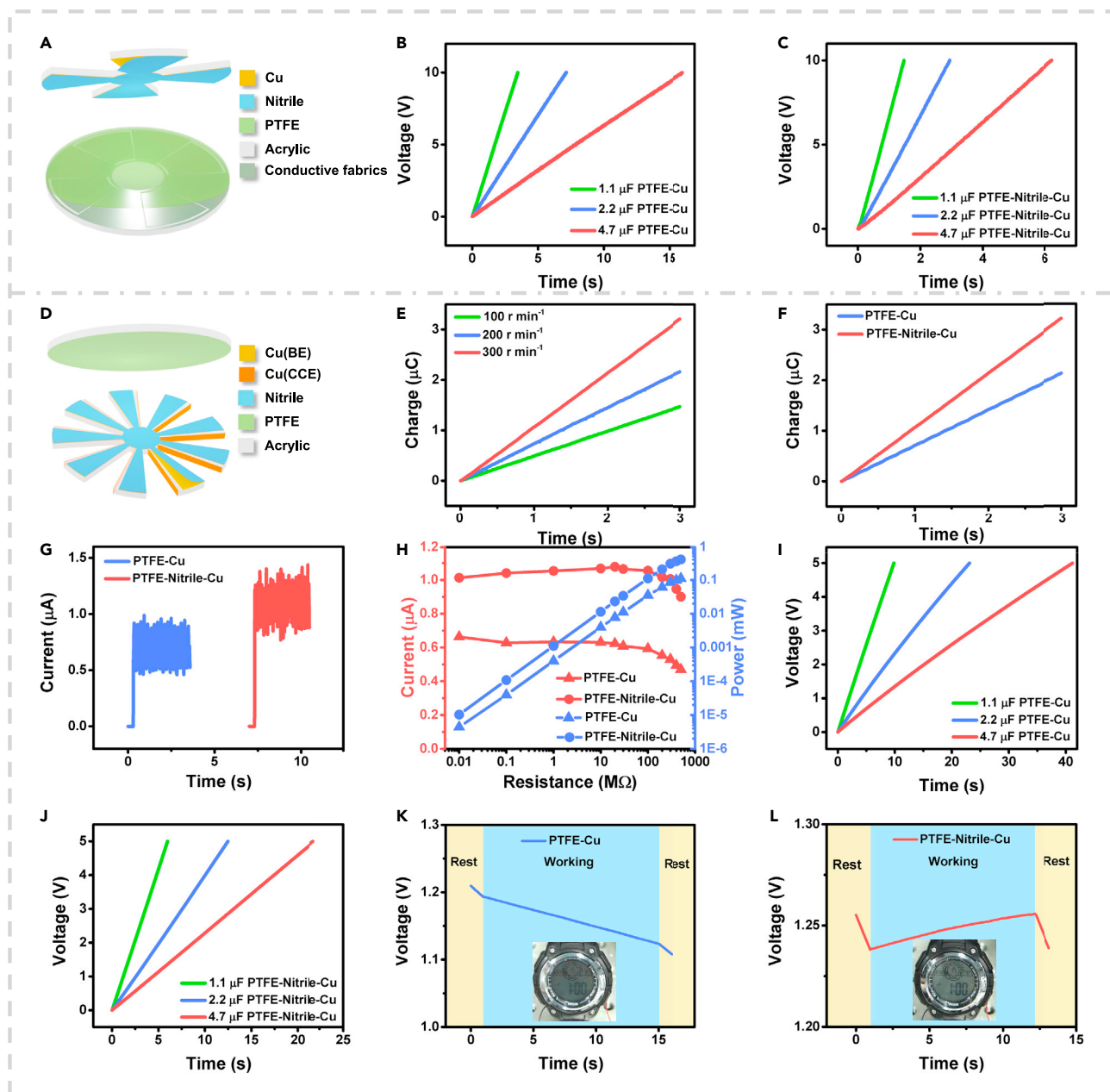


Figure 4. Output performance and application of rotary mode DE-TENGs

(A) Schematic illustration of rotary mode DEAC-TENG.

(B and C) Charging curves of capacitors with various capacitance by rotary mode AC-TENG (B) and DEAC-TENG (C).

(D) Schematic illustration of rotary mode DEDC-TENG.

(E) Output charge of rotary mode DEDC-TENG at different rotation rates.

(F and G) Output charge (F) and short-circuit current (G) comparison of rotary mode DC-TENG and DEDC-TENG.

(H) Output current and power comparison of rotary mode DC-TENG and DEDC-TENG.

(I and J) Charging curves of capacitors with varied capacitance by rotary mode DC-TENG (I) and DEDC-TENG (J).

(K and L) Charging curves of capacitors when the electronic calculator is driven by rotary mode DC-TENG (K) and DEDC-TENG (L).

from 100 r min^{-1} to 300 r min^{-1} , the transferred charge speed, the short-circuit current, and voltage of the device increased from 0.49 to $1.07 \mu\text{C s}^{-1}$, from 0.69 to $1.45 \mu\text{A}$, and from 60 to 134 V , respectively. Therefore, we compared output performance between rotary mode DC-TENG and rotary mode DEDC-TENG at 300 r min^{-1} .

min^{-1} . As depicted in [Figures 4F, 4G, and S10D](#), the transferred charge speed, the short-circuit current, and voltage of the rotary mode DEDC-TENG are all higher than those of the rotary mode DC-TENG, where the transferred charge speed increased by 51%. When connected to an external load, the current values of the two devices are almost stable and the power output improves linearly, with load resistance increasing from 0.01 to 500 M Ω . In particular, the maximum power of the rotary mode DEDC-TENG and rotary mode DC-TENG reaches 0.4 and 0.11 mW, respectively. The maximal power output of rotary mode DEDC-TENG increased by 2.6 times that of rotary mode DC-TENG ([Figure 4H](#)).

The most prominent feature of DC-TENG is the ability to charge energy-storage devices and drive electronics directly without any rectifier units. [Figures 4I and 4J](#) show the voltage curves of capacitors with capacitance of 1.1 μF , 2.2 μF , and 4.7 μF charged directly by a rotary mode DC-TENG and rotary mode DEDC-TENG without rectifier, and the corresponding circuit diagrams are shown in [Figures S9A and S9B](#). For charging 1.1 μF , 2.2 μF , and 4.7 μF capacitors to 5 V, the rotary mode DC-TENG takes 9.85 s, 23.11 s, and 41.17 s while the rotary mode DEDC-TENG takes 5.98 s, 12.48 s, and 21.8 s, respectively. The less charging time of the rotary mode DEDC-TENG indicates higher output performance of DEDC-TENG than that of DC-TENG. As an energy-harvesting device, DC-TENG can also drive electronics and charge energy-storage devices simultaneously. The self-powered system is built by integrating DC-TENG with the capacitor (47 μF) as energy-storage unit to power an electronic calculator. When powering the electronic calculator, the decreased voltage curve of the capacitor is monitored by a voltmeter as shown in [Figures 4K and 4L](#). As for the rotary mode DC-TENG, the curve slope decreases when the DC-TENG works and the calculator remains operational, while for the rotary mode DEDC-TENG the voltage of the capacitor increases once the device operates and the calculator still works simultaneously. These results further illustrate that the performance of DEDC-TENG is superior to that of DC-TENG.

Conclusions

In this work, the dielectric enhancement effect was firstly proposed to improve the performance of TENGs. It was demonstrated by dual-mode TENG that the dielectric enhancement method can simultaneously enhance the output performance of AC-TENG and DC-TENG. The universality of the dielectric enhancement layer for TENG was verified by comparison experiments for all types of TENGs. Besides, the dominate mechanism of the dielectric enhancement layer for improving the performance of TENGs is verified as the enhanced TE, and the principle of the dielectric enhanced DC-TENG producing continuous DC output is that the breakdown electrons pass through the nitrile film to the dielectric layer in the form of leakage current. Ultimately, a rotary mode DEAC-TENG and DEDC-TENG were fabricated to verify its ability for environmental energy collection, whereby the output power is 8.5- and 2.6-fold that of the rotary single dielectric layer TENG, respectively. Our work provides a simple and universal strategy for elevating the performance of all types of TENGs, which is beneficial to the promotion of large-scale energy harvesting by TENGs.

EXPERIMENTAL PROCEDURES

Resource availability

Lead contact

Further information and requests for resources and reagents should be directed to and will be fulfilled by the lead contact, Jie Wang (wangjie@binn.cas.cn).

Materials availability

The materials generated in this study are available from the lead contact upon reasonable request.

Data and code availability

The data used to support the findings of this study are available from the lead contact upon reasonable request.

Fabrication of dual-mode DE-TENG

Slider: (1) Cut a piece of acrylic sheet with dimensions of $20 \times 22 \times 5$ mm as substrate using a laser cutter. (2) Cut a piece of copper foil with dimensions of 20×22 mm and paste on the right of the substrate as BE. Cut a piece of copper foil with dimensions of 5×22 mm and paste on the right of the acrylic as CCE. There is a gap of about 0.7 mm between the BE and the CCE. (3) Cut a piece of nitrile with dimensions of 20×22 mm and place on the right of the copper foil as triboelectric layer. The gap between the nitrile and CCE is about 0.5 mm. Stator: (1) Cut a piece of acrylic sheet with dimensions of $66 \times 30 \times 5$ mm as substrate using a laser cutter. (2) Paste a piece of foam of the same size on the substrate to ensure sufficient contact. (3) Cut a piece of copper foil with dimensions of 33×30 mm as inductive electrode and paste it on the right of the foam. (4) Paste a piece of PTFE with dimensions of 66×30 mm on the top as triboelectric layer. (5) Connect both copper foils by wires for electrical measurement.

Fabrication of DEAC-TENG

CS-mode/SE-mode DEAC-TENG

Part I: (1) Cut a piece of acrylic sheet with dimensions of $20 \times 20 \times 5$ mm as substrate using a laser cutter. (2) Cut a piece of copper foil with dimensions of 20×20 mm and paste on the substrate as electrode. (3) Cut a piece of nitrile with dimensions of 20×20 mm and paste on the electrode as triboelectric layer. Part II: (1) Cut a piece of acrylic sheet with dimensions of $10 \times 10 \times 5$ mm as substrate using a laser cutter. (2) Cut a piece of foam with dimensions of 10×10 mm and paste on the substrate to ensure sufficient contact. (3) Cut a piece of copper foil with dimensions of 10×10 mm and paste on the foam as electrode. (4) Cut a piece of PTFE with dimensions of 10×10 mm and paste on the electrode as triboelectric layer. The CS-mode DEAC-TENG with TPU and nylon as the dielectric enhancement layers adopts the same method as that described for nitrile.

SFT-mode DEAC-TENG

Slider: (1) Cut a piece of acrylic sheet with dimensions of $20 \times 24 \times 5$ mm as substrate using a laser cutter. (2) Cut a piece of copper foil with dimensions of 20×24 mm and paste on the substrate as electrode. (3) Cut a piece of nitrile with dimensions of 20×24 mm and paste on the electrode as triboelectric layer. Stator: (1) Cut a piece of acrylic sheet with dimensions of $24 \times 50 \times 5$ mm as substrate by a laser cutter. (2) Cut a piece of foam with dimensions of 24×50 mm and paste on the substrate to ensure sufficient contact. (3) Cut two pieces of copper foil with dimensions of 24×25 mm and paste with small gap of 0.5 mm on the foam as electrode. (4) Cut a piece of PTFE with dimensions of 24×50 mm and paste on the electrode as triboelectric layer.

SL-mode DEAC-TENG

Slider: (1) Cut a piece of acrylic sheet with dimensions of $20 \times 24 \times 5$ mm as substrate using a laser cutter. (2) Cut a piece of copper foil with dimensions of 20×24 mm and paste on the substrate as electrode. (3) Cut a piece of nitrile with dimensions of $20 \times$

24 mm and paste on the electrode as triboelectric layer. Stator: (1) Cut a piece of acrylic sheet with dimensions of 30 × 35 × 5 mm as substrate using a laser cutter. (2) Cut a piece of foam with dimensions of 30 × 35 mm and paste on the substrate to ensure sufficient contact. (3) Cut a piece of copper foil with dimensions of 30 × 35 mm and paste on the foam as electrode. (4) Cut a piece of PTFE with dimensions of 30 × 35 mm and paste on the electrode as triboelectric layer.

Rotary mode DEAC-TENG

Stator: (1) Cut a disk-shaped acrylic sheet with dimensions of 70 mm as substrate using a laser cutter. (2) Paste a piece of foam of the same size on the substrate to ensure contact efficiency. (3) Cut a piece of conductive fabric with radical-arrayed sectors and the same central angle of 45° and paste on the foam. (4) Paste a piece of PTFE of the same size on the surface of conductive fabric as triboelectric layer. Rotator: (1) Cut a disk-shaped acrylic sheet with dimensions of 70 mm as substrate using a laser cutter, with radical-arrayed sectors and the same central angle of 45°. (2) Cut a piece of copper foil with the same shape as substrate and paste on the substrate. (3) Cut a piece of nitrile with the same shape as substrate and paste on the copper foil.

Fabrication of DEDC-TENG

DEDC-TENG

Slider: (1) Cut a piece of acrylic sheet with dimensions of 20 × 22 × 5 mm as substrate using a laser cutter. (2) Cut a piece of copper foil with dimensions of 20 × 22 mm and paste on the substrate as BE. Cut a piece of copper foil with dimensions of 5 × 22 mm and paste on the right of the acrylic as CCE. There is a gap of about 0.7 mm between the copper foil and the CCE. (3) Cut a piece of nitrile with dimensions of 20 × 22 mm and paste on the BE as triboelectric layer. The gap between the nitrile and CCE is about 0.5 mm. Stator: (1) Cut a piece of acrylic sheet with dimensions of 30 × 66 × 5 mm as substrate by a laser cutter. (2) Cut a piece of foam with dimensions of 30 × 66 mm and paste on the substrate to ensure sufficient contact. (3) Cut a piece of PTFE with dimensions of 30 × 66 mm and paste on the electrode as triboelectric layer. The DEDC-TENG with TPU and nylon as the dielectric enhancement layers adopts the same method as described for nitrile.

Rotary mode DEDC-TENG

Rotator: (1) Cut a disk-shaped acrylic sheet with dimensions of 70 mm as substrate using a laser cutter. (2) Paste a piece of foam of the same size on the substrate to ensure contact efficiency. (3) Paste a piece of PTFE of the same size on the surface of foam as triboelectric layer. Stator: (1) Cut a disk-shaped acrylic sheet with dimensions of 70 mm as substrate using a laser cutter, with radical-arrayed sectors and the same central angle of 20°. (2) Cut a piece of copper foil with the same shape as substrate and paste on the substrate. The copper foil should maintain a gap of about 0.7 mm from the sector margin. (3) Cut a piece of nitrile with the same shape as substrate and paste on the copper foil. The nitrile should maintain a gap of about 0.5 mm from the sector margin. (4) Cut nine pieces of copper foil with dimensions of 5 mm × 5.5 mm and paste them on the left of section in vertical direction, maintaining distance from nitrile and PTFE.

COMSOL simulation

The 2D potential distribution of dielectric enhancement layers was calculated using the commercial software COMSOL. For nitrile-PTFE condition, the surface charge density of PTFE is 90 $\mu\text{C m}^{-2}$. For TPU-PTFE condition, the surface charge density of PTFE is 81 $\mu\text{C m}^{-2}$. For nylon-PTFE condition, the surface charge density of PTFE is 79 $\mu\text{C m}^{-2}$.

Characterization and electrical measurement

The contact-separation and sliding process was driven by a linear motor (TSMV120-1S). The rotary process was operated by a rotational motor (80BL165S75-3130TK0). The short-circuit current, voltage, and transferred charges of the TENG were measured by a programmable electrometer (Keithley model 6514). A potentiostat (VSP-300, Bio-Logic, France) was used to test the capacitance of the capacitor and the charge/discharge curves of the self-charging power system. The leakage current of nitrile was measured by a capacitor leakage current/IR meter (TH2689).

SUPPLEMENTAL INFORMATION

Supplemental information can be found online at <https://doi.org/10.1016/j.matt.2021.10.019>.

ACKNOWLEDGMENTS

Research was supported by the National Key R & D Project from the Minister of Science and Technology (2016YFA0202701), Beijing Municipal Science and Technology Commission (Z171100000317001, Z171100002017017, Y3993113DF), and National Natural Science Foundation of China (grant no. 61774016, 51432005, 5151101243, 51561145021).

AUTHOR CONTRIBUTIONS

Conceptualization, S. Cui, L.Z., D.L., Z.L.W., and J.W.; methodology, S. Cui, L.Z., and D.L.; investigation, S. Cui, L.Z., D.L., S.L., L.L., S. Chen, Z.Z., and W.Y.; writing – original draft, S. Cui, L.Z., and D.L.; writing – review & editing, Z.L.W. and J.W.; funding acquisition, Z.L.W. and J.W.; resources, Z.L.W. and J.W.; supervision, Z.L.W. and J.W.

DECLARATION OF INTERESTS

The authors declare no competing interests.

Received: April 22, 2021

Revised: July 3, 2021

Accepted: October 17, 2021

Published: November 9, 2021

REFERENCES

1. Wang, Z.L. (2019). Entropy theory of distributed energy for internet of things. *Nano Energy* 58, 669–672.
2. Fan, F.-R., Tian, Z.-Q., and Wang, Z.L. (2012). Flexible triboelectric generator! *Nano Energy* 1, 328–334.
3. Wang, Z.L. (2014). Triboelectric nanogenerators as new energy technology and self-powered sensors—principles, problems and perspectives. *Faraday Discuss* 176, 447–458.
4. Zhou, L., Liu, D., Wang, J., and Wang, Z.L. (2020). Triboelectric nanogenerators: fundamental physics and potential applications. *Friction* 8, 481–506.
5. Liu, D., Zhou, L., Wang, Z.L., and Wang, J. (2021). Triboelectric nanogenerator: from alternating current to direct current. *iScience* 24, 102018.
6. Wang, Z.L., Chen, J., and Lin, L. (2015). Progress in triboelectric nanogenerators as a new energy technology and self-powered sensors. *Energy Environ. Sci.* 8, 2250–2282.
7. Wang, Z.L. (2020). On the first principle theory of nanogenerators from Maxwell's equations. *Nano Energy* 68, 104272.
8. Wu, C., Wang, A.C., Ding, W., Guo, H., and Wang, Z.L. (2019). Triboelectric nanogenerator: a foundation of the energy for the new era. *Adv. Energy Mater.* 9, 1802906.
9. Cheng, T., Gao, Q., and Wang, Z.L. (2019). The current development and future outlook of triboelectric nanogenerators: a survey of literature. *Adv. Mater. Technol.* 4, 1800588.
10. Peng, J., Kang, S.D., and Snyder, G.J. (2017). Optimization principles and the figure of merit for triboelectric generators. *Sci. Adv.* 3, eaap8576.
11. Jiang, C., Dai, K., Yi, F., Han, Y., Wang, X., and You, Z. (2018). Optimization of triboelectric nanogenerator load characteristics considering the air breakdown effect. *Nano Energy* 53, 706–715.
12. Wang, J., Wang, C., Dai, Y., Zhao, Z., Wang, A., Zhang, T., and Wang, Z.L. (2017). Achieving ultrahigh triboelectric charge density for efficient energy harvesting. *Nat. Commun.* 8, 88.
13. Wang, J., Li, S., Yi, F., Zi, Y., Lin, J., Wang, X., Xu, Y., and Wang, Z.L. (2016). Sustainably powering wearable electronics solely by biomechanical energy. *Nat. Commun.* 7, 12744.
14. Wang, S., Xie, Y., Niu, S., Lin, L., Liu, C., Zhou, Y., and Wang, Z.L. (2014). Maximum surface charge density for triboelectric nanogenerators achieved by ionized-air injection: methodology and theoretical understanding. *Adv. Mater.* 26, 6720–6728.

15. Chen, A., Zhang, C., Zhu, G., and Wang, Z.L. (2020). Polymer materials for high-performance triboelectric nanogenerators. *Adv. Sci.* *7*, 2000186.
16. Zhang, C., Zhou, L., Cheng, P., Yin, X., Liu, D., Li, X., Guo, H., Wang, Z.L., and Wang, J. (2020). Surface charge density of triboelectric nanogenerators: theoretical boundary and optimization methodology. *Appl. Mater. Today* *18*, 100496.
17. Xu, L., Bu, T., Yang, X., Zhang, C., and Wang, Z.L. (2018). Ultrahigh charge density realized by charge pumping at ambient conditions for triboelectric nanogenerators. *Nano Energy* *49*, 625–633.
18. Liu, W., Wang, Z., Wang, G., Liu, G., Chen, J., Pu, X., Xi, Y., Wang, X., Guo, H., Hu, C., and Wang, Z.L. (2019). Integrated charge excitation triboelectric nanogenerator. *Nat. Commun.* *10*, 1426.
19. Liu, Y., Liu, W., Wang, Z., He, W., Tang, Q., Xi, Y., Wang, X., Guo, H., and Hu, C. (2020). Quantifying contact status and the air-breakdown model of charge-excitation triboelectric nanogenerators to maximize charge density. *Nat. Commun.* *11*, 1599.
20. Li, Y., Zhao, Z., Liu, L., Zhou, L., Liu, D., Li, S., Chen, S., Dai, Y., Wang, J., and Wang, Z.L. (2021). Improved output performance of triboelectric nanogenerator by fast accumulation process of surface charges. *Adv. Energy Mater.* *11*, 2100050.
21. Liu, D., Yin, X., Guo, H., Zhou, L., Li, X., Zhang, C., Wang, J., and Wang, Z.L. (2019). A constant current triboelectric nanogenerator arising from electrostatic breakdown. *Sci. Adv.* *5*, eaav6437.
22. Zhao, Z., Dai, Y., Liu, D., Zhou, L., Li, S., Wang, Z.L., and Wang, J. (2020). Rationally patterned electrode of direct-current triboelectric nanogenerators for ultrahigh effective surface charge density. *Nat. Commun.* *11*, 6186.
23. Liu, D., Zhou, L., Li, S., Zhao, Z., Yin, X., Yi, Z., Zhang, C., Li, X., Wang, J., and Wang, Z.L. (2020). Hugely enhanced output power of direct-current triboelectric nanogenerators by using electrostatic breakdown effect. *Adv. Mater. Technol.* *5*, 2000289.
24. Yi, Z., Liu, D., Zhou, L., Li, S., Zhao, Z., Li, X., Wang, Z.L., and Wang, J. (2021). Enhancing output performance of direct-current triboelectric nanogenerator under controlled atmosphere. *Nano Energy* *84*, 105864.
25. Zhou, L., Liu, D., Zhao, Z., Li, S., Liu, Y., Liu, L., Gao, Y., Wang, Z.L., and Wang, J. (2020). Simultaneously enhancing power density and durability of sliding-mode triboelectric nanogenerator via interface liquid lubrication. *Adv. Energy Mater.* *10*, 2002920.
26. Zhou, L., Liu, D., Li, S., Zhao, Z., Zhang, C., Yin, X., Liu, L., Cui, S., Wang, Z.L., and Wang, J. (2020). Rationally designed dual-mode triboelectric nanogenerator for harvesting mechanical energy by both electrostatic induction and dielectric breakdown effects. *Adv. Energy Mater.* *10*, 2000965.
27. Chen, J., Guo, H., He, X., Liu, G., Xi, Y., Shi, H., and Hu, C. (2016). Enhancing performance of triboelectric nanogenerator by filling high dielectric nanoparticles into sponge PDMS film. *ACS Appl. Mater. Inter.* *8*, 736–744.
28. Dzhardimalieva, G.I., Yadav, B.C., Lifintseva, T.y.V., and Uflyand, I.E. (2021). Polymer chemistry underpinning materials for triboelectric nanogenerators (TENGs): recent trends. *Eur. Polym. J.* *142*, 110163.